DOI 10.7343/as-2025-917

ACQUE SOTTERRANEE
Italian Journal of Groundwater

2025-AS55-917: 53 - 67

journal homepage: https://www.acquesotterranee.net/

Assessment of groundwater influenced by seawater using geochemical modeling and statistical analysis: Basrah Province, Iraq

Valutazione dell'influenza dell'acqua marina sulle acque sotterranee attraverso modellazione geochimica e analisi statistica: Provincia di Bassora, Iraq

Lamees AL-QURNAWY[a], **Wisam MUTTASHAR**[a], **Ali AL-NASRAWI**[b]

[a] Department of Marine Geology, Marine Science Center, University of Basrah, Basrah-Iraq. Email : *lamees.abdulhussein@uobasrah.edu.iq*
[b] Department of Geography, University of Babylon, Babylon-Iraq

ARTICLE INFO

Ricevuto/*Received*: 27 July 2025
Accettato/*Accepted*: 10 December 2025
Pubblicato online/*Published online*: 30 December 2025

Handling Editor:
Silvia Bertoldo

Citation:
Al-Qurnawy, L., Muttashar, W., Al-Nasrawib, A. (2025). Assessment of groundwater influenced by seawater using geochemical modeling and statistical analysis: Basrah Province, Iraq.
Acque Sotterranee - *Italian Journal of Groundwater*, 14(4), 53 - 67
https://doi.org/10.7343/as-2025-917

Correspondence to:
Lamees Al-Qurnawy
lamees.abdulhussein@uobasrah.edu.iq

Keywords:
coastal aquifers, Piper, Schoeller, saturation index, cluster analysis.

Parole chiave:
acquiferi costieri, diagramma di Piper, diagramma di Schoeller, indice di saturazione, analisi di clustering gerarchico.

Abstract

Seawater intrusion in coastal aquifers is a complicated phenomenon that requires a practical framework to assess the constituents' groundwater source. The current paper focuses on the processes influencing coastal groundwater in the southeastern region of Basrah, southern Iraq. Thirteen groundwater samples were subjected to comprehensive hydrogeochemical treatments, including hydrogeochemical analysis with Piper, Schoeller, and Gibbs plots, geochemical modeling, and statistical analysis supported by hierarchical cluster analysis. The results of the Piper plot indicated that the analyzed groundwater is characterized as Na-Cl (77%) and Ca-Mg-Cl (23%) and belongs to the order of Cl^- > Na^+ > SO_4^{2-} > Ca^{2+} > Mg^{2+} > HCO_3^- as identified by Schoeller results. Gibbs' plot results indicated the processes of evaporation and seawater dominance. Saturation indices of minerals in groundwater revealed a slight supersaturation (SI > 0) with calcite and dolomite, suggesting limited precipitation of carbonate minerals. In contrast, gypsum and anhydrite showed a slight undersaturation (SI < 0), indicating minimal dissolution of evaporite minerals, while halite and sylvite minerals suggested a strong undersaturation (SI < 0), reflecting that dissolution of salts is a common process in the coastal areas. Furthermore, cluster analysis demonstrated that the ionic content of groundwater was significantly affected by seawater, evaporation processes, and minimal sedimentation of carbonate minerals. These techniques are recommended for controlling the groundwater extraction within the study area.

Riassunto

L'intrusione marina negli acquiferi costieri è un fenomeno complesso che richiede un approccio metodologico efficace per valutare l'origine e la composizione delle acque sotterranee. Il presente studio analizza i processi che influenzano le acque sotterranee costiere nella regione sud-orientale di Bassora, Iraq meridionale.
Tredici campioni di acqua sotterranea sono stati sottoposti a una valutazione idrogeochimica completa, comprendente analisi tramite i diagrammi di Piper, Schoeller e Gibbs, modellazione geochimica con gli indici di saturazione e analisi statistica supportata da analisi gerarchica dei cluster. I risultati del diagramma di Piper hanno evidenziato che le acque sotterranee analizzate si inquadrano prevalentemente nelle facies idrochimiche Na–Cl (77%) e Ca–Mg–Cl (23%). Inoltre, in accordo con il diagramma di Schoeller, la sequenza di dominanza ionica è risultata essere Cl^- > Na^+ > SO_4^{2-} > Ca^{2+} > Mg^{2+} > HCO_3^-. I diagrammi di Gibbs hanno indicato che i processi dominanti sono l'evaporazione e l'intrusione marina. Gli indici di saturazione hanno evidenziato una lieve sovrasaturazione (SI > 0) di calcite e dolomia, suggerendo una precipitazione limitata di minerali carbonatici; al contrario, gesso e anidrite risultano leggermente sottosaturi (SI < 0), indicando una dissoluzione minima di minerali evaporitici, mentre halite e silvite mostrano una marcata sottosaturazione (SI < 0), evidenziando che la dissoluzione dei sali sia un processo comune nelle aree costiere. Inoltre, l'analisi di clustering gerarchico ha evidenziato che il contenuto ionico delle acque sotterranee è fortemente influenzato dall'intrusione marina, dai processi evaporativi e da una limitata sedimentazione di minerali carbonatici. Le tecniche adottate sono raccomandate come strumenti di supporto per la gestione e il controllo dello sfruttamento delle acque sotterranee nell'area di studio.

Introduction

In general, most aquifers that provide groundwater are affected by continuous depletion. In arid regions with limited rainfall, a lot of groundwater is consumed for irrigation of agricultural lands and to supply water for industrial sites. In coastal areas, overexploitation of groundwater results in declining water levels and increasing salinization which poses a significant risk to agricultural lands (El-Rawy et al., 2023). However, this salinity can be flushed out in cases of heavy rainfall that recharges the aquifer (Samsudin et al., 2008). One of the challenges to assess water salinity is predicting the origin of salts and the chemical processes that influence the water quality. According to McArthur et al. (1989), sources of salinity represent marine-origin water, seawater trapped in inland basins due to marine regressions, periodic marine salt aerosols, and decomposition of evaporite and carbonate minerals by weathering (Sarikhani et al., 2015). In addition, human activities, agricultural practices, natural weathering processes, biogeochemical interactions are considered affecting sources (Kanagaraj et al., 2018). Near the coastal area, seawater is the primary cause of salinization in unconfined aquifers, whereas confined aquifers experience water–rock interactions and mixing with other water sources (Hasan et al., 2023). Moreover, the presence of seawater intrusion originates from various conditions, including low infiltration, excessive pumping, gentle hydraulic gradients, tidal and estuarine activity, and local hydrogeological conditions (Chandrasekar et al., 2014). In fact, coastal groundwater systems are consistently affected by sea level rise, tidal flooding, recurrent cyclonic storms, and climate change, leading to unique challenges concerning groundwater sustainability in coastal zones (Mohanty & Rao, 2019). However, seawater and groundwater differ significantly in their chemical composition; seawater is predominantly composed of chloride and sodium (84%), while calcium and bicarbonate are the dominant ions in groundwater (Tomaszkiewicz et al., 2014). Generally, determining groundwater influenced by seawater is highly challenging due to the hydrogeological complexity in the coastal areas (Aladejana et al., 2021).

With regard to the investigated area, groundwater is a critical resource for industrial and agricultural activities, besides other purposes; and the uncontrolled overexploitation may deteriorate the quality of water. Jassim & Joff (2006) mentioned that overproduction from aquifer may cause inland movement of seawater through sediments of the Arabian Gulf. It is worth noting that earlier works on Dibdibba aquifer in Basrah City have provided extensive insights into the hydrogeochemical characteristics. Haddad and Hawa (1979), conducted hydrological assessment in Safwan area southern Iraq, offering fundamental investigation on groundwater conditions including chemical parameters and hydraulic properties of aquifer. Al-Jawad et al. (1989) explored aquifer characteristics through the data of pumping test from large-diameter wells. Al-Kubaisi (1996 and 1999) inspected the hydrogeological setting of aquifer in Safwan-Zubair area; he analyzed the water budget and explored hydrochemical properties of groundwater. Atiaa (2000) suggested numerical models for detecting the hydraulic properties applying pumping tests. Ghalib (2000) further studied the hydrogeochemical modeling to assess the quality of groundwater under the impact of pumping. The influence of artificial recharge on water quality was investigated by Ghalib (2008), providing insights into aquifer responses to recharge practices. Furthermore, Al-Sudani (2019), studied the groundwater system of Dibdibba aquifer, Al-Abadi and Al-Qurnawy (2021) applied decision making techniques to assess the groundwater rising. AlMallah et al. (2022) carried out water quality from a statistical point of view. Al-Qurnawy et al. (2024) focused on groundwater quality in terms of drinking and irrigation suitability. Recently, the hydrogeochemical studies on saltwater intrusion within Dibdibba groundwater have been investigated by researchers (Al-Musawi & Khorshid, 2013, Al-Suraifi 2015, Abdulameer et al., 2018, Abdulameer et al., 2021, Alqurnawy et al., 2022, Al-Qurnawy et al., 2023). However, this work applies geochemical modeling and minerals behavior and also presents a new statistical clustering method that has not been used before on Dibdibba aquifer as relevant to seawater intrusion. It provides a robust framework to understand complex hydrogeochemical interactions in the Dibdibba aquifer, emphasizing the need for sustainable groundwater policies in arid coastal regions.

Study area

The sampled water within the study area is located in the eastern sector of Zubair district, adjacent to the marine Khor Al-Zubair channel, approximately 55 km from the Arabian Gulf from the area located within 29°59' to 30°15'N and 47°42' to 48°1'E, covering a total of 438.68 km² (Fig. 1). The study area is part of Al-Batin alluvial fan deposits, one of the largest sedimentary fans in Iraq, particularly within the southern Iraqi desert region (Sissakian et al., 2014) and is mainly covered with gravelly sand and sandy gravel, as displayed from the geological map (Fig. 2). It extends from the southwestern section near the Iraq-Kuwait border, toward northeastward, where it is deposited on the top of the Dibdibba Formation (Al-Kubaisi, 1996). The Khor Al-Zubair estuary is characterized by hyper-saline, shallow waters and serves as a conduit connecting to the Arabian Gulf. The Khor Al-Zubair channel is characterized by estuarine lagoon and it is significantly influenced by strong tidal currents (Al-Ramadhan et al., 1988). On the eastern side of the Khor Al-zubair channel, the formation is covered up by fluvio-estuarine deposits extending to the Iraqi muddy coast at the head of the Arabian Gulf comprising clay, silt, and a minor sand content (Muttashar et al., 2024). Table 1 displays the stratigraphic sequence of the study area. The oldest Dibdibba Formation historically ranged from the Pliocene to the Pleistocene; it was deposited in an alluvial delta environment and is covered by the Quaternary deposits (Jassim & Joff, 2006). The Quaternary deposits range from the Pleistocene to the Holocene, with a thickness not exceeding 300 feet (Al-

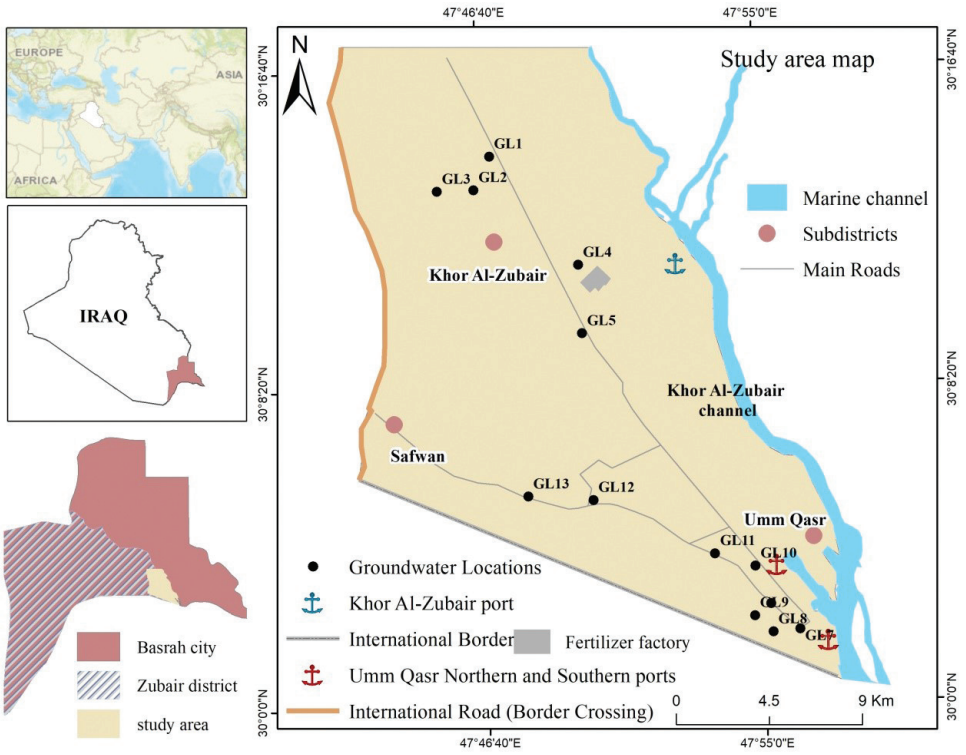

Fig. 1 - Geographical location map of the study area.

Fig. 1 - Carta di localizzazione dell'area di studio.

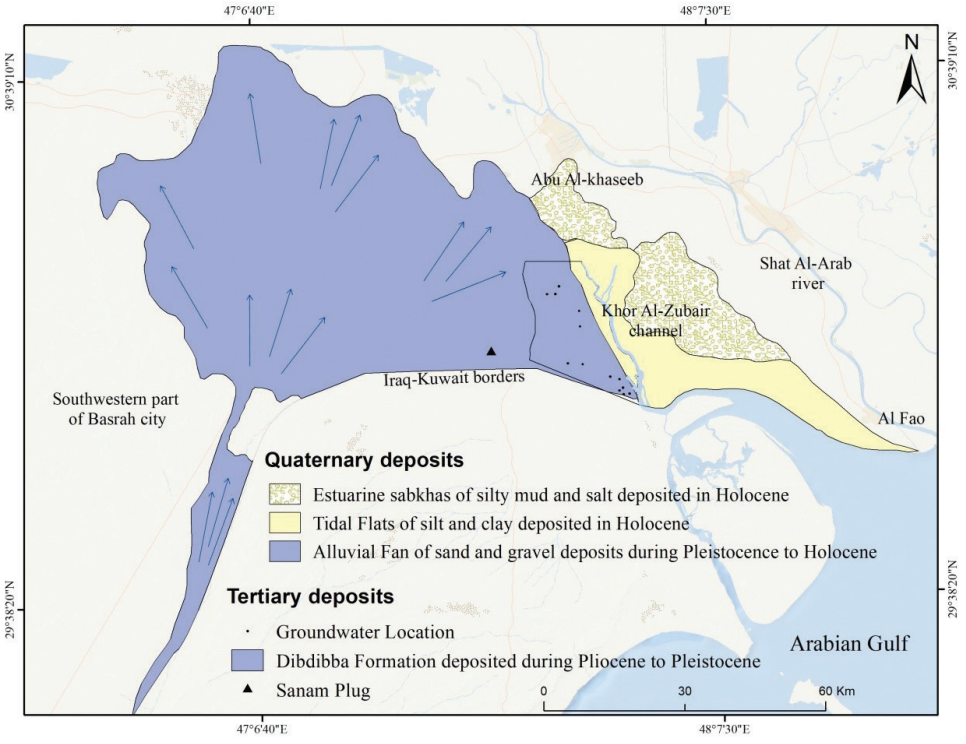

Fig. 2 - Geological map of the study area. (Source: Sissakian & Fouad, 2015)

Fig. 2 - Carta geologica dell'area di studio. (da: Sissakian & Fouad, 2015).

Naqib, 1967). This area is characterized by marine sediments represented by brackish to estuarine deposits (Buday, 1980). Tectonically, the entire area is located within the unstable shelf of the Mesopotamian zone within Basrah block.

Based on the hydrogeological setting, the aquifer is situated within Dibdibba Formation and Quaternary deposits, including two parts of the water-bearing layer, upper and lower: the upper is shallow brackish unconfined aquifer that has salinity less than 10000 mg/l, while lower is deeper saline confined to semi-confined aquifer exceeding 10000 mg/l in most areas (Al-Kubaisi, 1999). They are distinguished by the Jojab layer of hard clay which reaches up to 2 m in thickness,

Tab. 1 - Stratigraphic sequence in the study area.

Tab. 1 - Sequenza stratigrafica nell'area di studio.

Geological unit	Quaternary Deposits (of the mesopotamian plain)
Age	Pleistocene- Holocene (Al-Naqib, 1967)
Thickness	>300 feet (Al-Naqib, 1967); 150-200 m (Buday, 1980)
Lithology	Gravels, sands, silts, and clay (Buday, 1980)
Environment	Deltaic, lacustrine, fluviatile sediments (Buday, 1980)
Geological unit	**Dibdibba Formation**
Age	Pliocene-Pleistocene (Al-Naqib, 1967)
Thickness	1160 feet about 354 m (Al-Naqib, 1967)
Lithology	Sandstone and gravel (Sissakian and Mohammed, 2007)
Environment	Fluvial sedimentation, alluvial fans (Sissakian and Mohammed, 2007)

has a hydraulic conductivity of 0.38 m/d (Al-Kubaisi, 1996) and is located at approximately 27 m in depth (Abdulameer et al., 2018). According to Jassim and Goff (2006), unusually salinity found in certain groundwater near the recharge zone indicated localized leakage from deeper aquifers. Based on earlier investigations Haddad and Hawa (1979), Al-Jawad (1989), Al-Kubaisi (1996), Atiaa (2000) and as reported by Atiaa and Al-Asadiy (2007), the transmissivity of the aquifer was estimated to exceed 300 m²/d and average of saturated thickness approximately included 14 m, while hydraulic conductivity scored 20 m/d. The regional groundwater flow is directed toward the northeastern parts, originating from the southwest and moving toward the discharge zones along the Euphrates River, Hor Al-Hammar, and the Shatt Al-Arab (Al-Jiburi and Al-Basrawi, 2009). The study area is located in Basrah , which is characterized by an arid and semi-arid regions with extremely high summer temperatures, mild winters, very low rainfall, and intense evaporation. The annual average rainfall is around 134 mm with an annual average temperature 26.1C°, while evaporation exceeds 3220 mm/year due to strong solar heating. Average wind speeds are around 5.3 m/s within Basrah station (Hassan, 2025).

Based on the Shuttle Radar Topography Mission data (SRTM), the topographic elevation of the study area ranges from sea level near the coasts to approximately 62 meters above sea level (Fig. 3a). The groundwater depths reached from 2.64 m to 18.6 m as shown in (Fig. 3b). These depths were measured in the field through the same period of the sampling.

Material and Methods

Sampling

The current study included data from 13 water samples labeled GL1 to GL13 which represent a part of earlier investigations (Alqurnawy et al., 2022, Al-Qurnawy et al., 2023) that were taken during the winter of January 2021. Water-well sampling was conducted from Khor Al-Zubair to Umm Qasr and the main road of Safwan-Umm Qasr, including sample collection and measurement of electrical conductivity (EC) using an inoLab Con 720 conductivity meter (WTW GmbH) as well as groundwater depth using

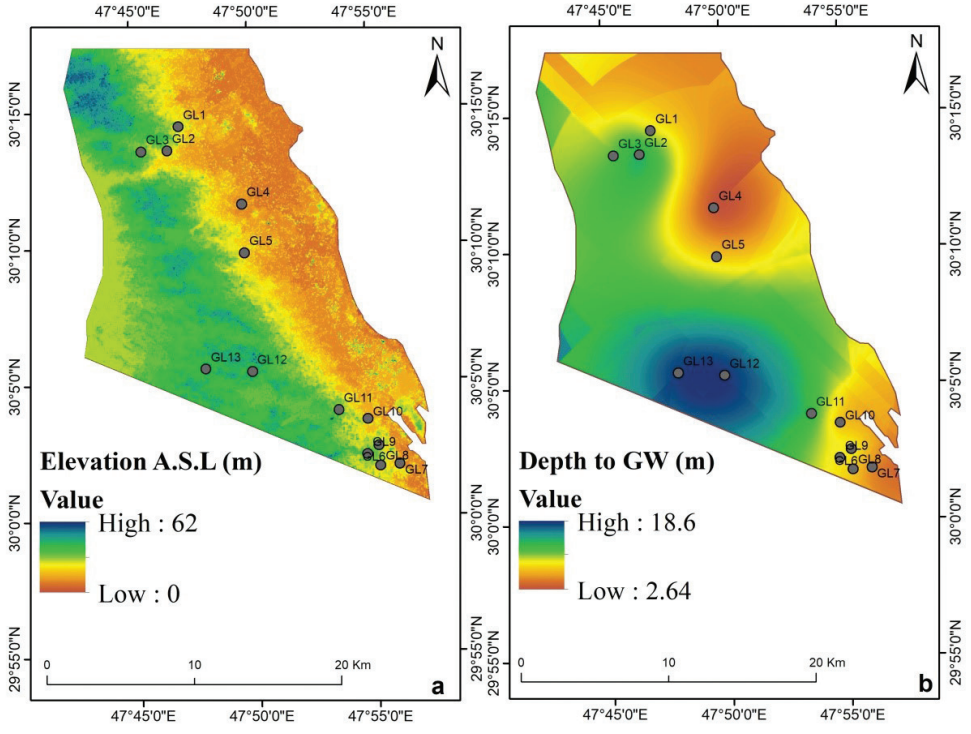

Fig. 3 - Spatial distribution (a) Elevation of earth surface, and (b) Depth to groundwater.

Fig. 3 - Distribuzione spaziale (a) della quota della superficie terrestre and (b) della profondità della falda.

Heron Water Tape water level meter (Heron Instruments, Inc.). The chemical analyses of the samples included pH and major ions. Calcium (Ca^{2+}) and magnesium (Mg^{2+}) were determined using a volumetric titration method with EDTA in the Quality Control Laboratory of Basrah Water Directorate; sodium (Na^{+}) and potassium (K^{+}) were measured in the Geochemical Laboratory of Marine Science Center employing flame photometer; chloride (Cl^{-}) and bicarbonate (HCO_3^{-}) were determined in the Geochemical Laboratory using titration method (Mohr method for determining chloride and acid titration with HCl for bicarbonate); sulfate (SO_4^{2-}) was analyzed in the Iraq Group for Science Laboratory of Marine Science Center applying ultraviolet visible spectrophotometer turbidimetric method, and nitrate (NO_3^{-}) was measured in the Quality Control Laboratory by Prime Lab Spectrophotometric device based on wavelength detection. The total dissolved solids (TDS) were recalculated using Diagrammes software instead of the empirical equation (EC * 0.64) that was used in earlier investigations for supporting the validity of the updated method. In this method, Diagrammes software automatically calculates TDS values from entered major cations and anions.

Analytical software

The Geographical Information System ArcGIS software (Version 10.8) was applied for delineating thematic and spatial distribution maps including the site map of the selected area and the geological, surface elevation and depth to groundwater maps. The elevation map represents the Digital Elevation Model (DEM) with 30 m resolution downloaded from the United States of the Geological Survey (USGS). The flowchart of methodology is illustrated in (Fig. 4). Groundwater physicochemical data were applied in GIS for extracting the spatial distribution maps of mineralization, total dissolved solids, and the saturation index of minerals through the Kriging geostatistical analysis tool and the IDW interpolation tool. The Diagrammes software (Version 6.77; Simler, 2009) was utilized to generate the hydrochemical facies Piper and Schoeller diagrams, while geochemical modeling was carried out using PHREEQC Interactive software (Version 3.7.3; Parkhurst and Appelo, 2013) developed by the U.S. Geological Survey to determine the saturation indices of minerals in the groundwater. Furthermore, IBM SPSS Statistics (Version 25; IBM Corp, Armonk, NY, USA) facilitated the creation of box plot and the statistical clustering analysis as dendrograms for detecting the relationship among the ionic clusters. During dendrograms construction, rows of samples (cases) and columns of physicochemical parameters (variables) had been standardized by Z scores to ensure uniform units. The ward linkage method, measured by squared Euclidean distance, was selected for that purpose. It is essential procedure to aggregate the sampled water in terms of physicochemical proximity and similarity.

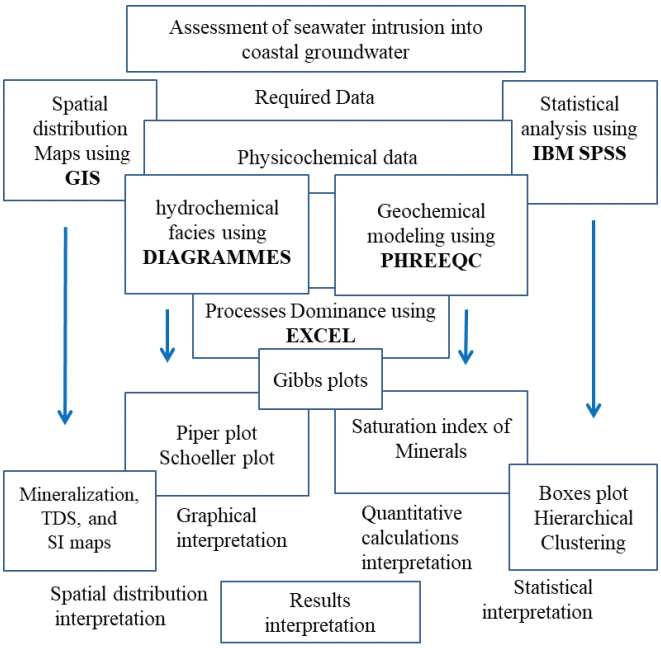

Fig. 4 - Flowchart of methodology applied on the study area.

Fig. 4 - Diagramma di flusso della metodologia applicata all'area di studio.

Results and discussion

Physical and chemical analyses

This study comprised the analyzed physicochemical characteristics including major positive ions (Ca^{2+}, Mg^{2+}, Na^{+}, K^{+}), major negative ions (Cl^{-}, SO_4^{2-}, HCO_3^{-}), and minor anion NO_3^{-} and other water quality indicators such as EC, TDS, pH, and total hardness (TH), as summarized in (Table 2). The values are presented in terms of maximum, 75th percentile, median, 25th percentile, and minimum levels in the boxes plot as shown in Figure 5. The EC ranged from 4920 to 18400 µS/cm, with the mean value of 11180 µS/cm, while TDS from 3482 to 13400 mg/L, with a mean value of 7776.6 mg/L. The higher TDS can be attributed to the contribution of salts from the subsurface lithology, as well as the extended residence time of groundwater in contact with the aquifer body (Selvam et al., 2013). The pH considers the scale of acidity and alkalinity in a solution; it differed from 6.95 to 7.25; the average was 7.15, suggesting minimum alkalinity. The TH as CaCO3 varied from 1969.8 to 4188.78 mg/L, averaging 2682.58 mg/L. Ca^{2+}concentration ranged from 395 to 842 mg/L (mean 537.5 mg/L), and Mg^{2+} from 239 to 507 mg/L (mean 325.8 mg/L). The detrital plagioclase and feldspar are considered the main source of Ca^{2+} and Mg^{2+}, as well as sedimentary rocks like limestone, dolomite, gypsum, anhydrite, and clay minerals found in the coastal region (Chandrasekar et al., 2014). The Na^{+} ranged from 298 to 3620 mg/L, averaging 1701 mg/L. The high Na^{+} in groundwater is influenced by multiple factors, including seawater intrusion, halite dissolution, and rock-water interactions in the aquifer (Mohanty & Rao, 2019). Levels of K^{+} vary from 11.4 to 26.5 mg/L, with a mean value of 17.7 mg/L. The Cl^{-} differed from 595.6 to 4766 mg/L; the

Tab. 2 - The descriptive statistics of the analyzed groundwater.

Tab. 2 - Parametri statistici descrittivi delle acque sotterranee analizzate.

Properties	Mean	Median	S.D	Minimum	Maximum
EC (µS/cm)	11180	10300	4715.9	4920	18400
TDS (mg/L)	7776.6	7401	3194.1	3482	13400
pH	7.15	7.19	0.10	6.95	7.25
TH (mg/L)	2682.58	2383.68	747.06	1969.8	4188.78
Ca^{2+} (mg/L)	537.5	480	150.1	395	842
Mg^{2+} (mg/L)	325.8	290	90.5	239	507
Na^{+} (mg/L)	1701	1500	1048.8	298	3620
K^{+} (mg/L)	17.7	17.5	4.29	11.4	26.5
Cl^{-} (mg/L)	2138.90	1787.7	1362.2	595.6	4766
SO_4^{2-} (mg/L)	2827.3	2867	685.65	1732.4	3888.5
HCO_3^{-} (mg/L)	227.6	189.3	100.33	103.7	433
NO_3^{-} (mg/L)	0.85	0.84	0.30	0.48	1.19

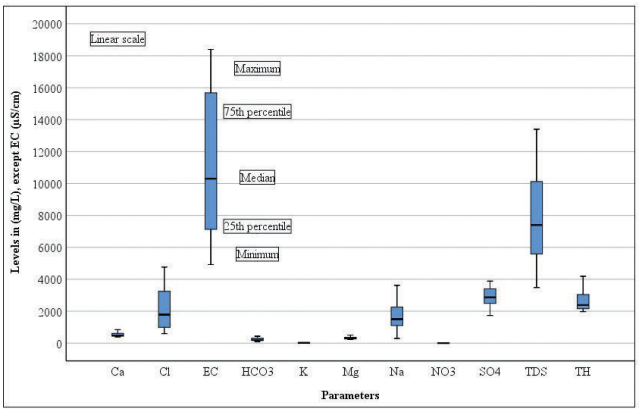

Fig. 5 - Box plot of physicochemical parameters in groundwater samples.

Fig. 5 - Box plot dei parametri fisico-chimici nei campioni di acqua sotterranea.

average was 2138.90 mg/L. The primary source of Cl^{-} in the Earth's crust is the mineral halite, found in the evaporite deposits, which developed over the geological time through the evaporation of seawater (Sarikhani et al., 2015). High Cl^{-} concentrations in groundwater are mainly due to the seawater mixing, particularly near the coasts and in areas affected by seawater intrusion or upconing of deeper saline groundwater from overexploitation (Alfarrah & Walraevens, 2018). Aladejana et al. (2021) noted that the presence of Cl^{-} may result from both anthropogenic sources, such as sewage effluent or leachates. The SO_4^{2-} varied from 1732.4 to 3888.5 mg/L, mean 2827.3 mg/L. High levels of sulfate are mostly associated with Cl^{-} concentrations from seawater intrusion and deep saline water upconing; other sources of $SO42^{-}$ come from gypsum and anhydrite dissolution (Alfarrah & Walraevens, 2018). The HCO_3^{-} differed from 103.7 to 433.1 mg/L, with a mean value of 227.6 mg/L, indicating carbonates weathering. The NO_3^{-} varied from 0.48 to 1.19 mg/L; the average was 0.85 mg/L; potential sources of NO_3^{-} include agricultural fertilizers and pesticides (Ardjane et al., 2025).

Data quality

The precision of chemical analyses had been evaluated by calculating the ionic balance error (IBE), as outlined by (Appelo & Postma, 2004). This method considers the total cations (positive charges) and total anions (negative charges) in the analyzed water (Equation 1). Table 3 shows the error levels and accuracy of the groundwater samples. Samples with accuracy below 90% were excluded from the analysis. Consequently, the chemical data of the groundwater samples were considered to be reliable for water chemistry analyses and geochemical modeling.

$$IBE = \frac{\left|(\Sigma cations) - (\Sigma anions)\right|}{(\Sigma cations) + (\Sigma anions)} \cdot 100 \quad (1)$$

Tab. 3 - Calculation of ionic balance error for cations and anions (meq/L).

Tab. 3 - Calcolo dell'errore di bilancio ionico per cationi e anioni (meq/L).

Wells	Sub-district	Σ Cation	Σ Anions	IBE %	Accuracy 100-IBE
GL1	Khor Al-Zubair	56.61	58.32	1.48	99
GL2	Khor Al-Zubair	52.85	56.29	3.15	97
GL3	Khor Al-Zubair	113.38	118.84	2.35	98
GL4	Khor Al-Zubair	169.92	188.93	5.29	95
GL5	Khor Al-Zubair	95.13	105.85	5.33	94
GL6	Umm-Qasr	89.25	85.08	2.49	98
GL7	Umm-Qasr	169.48	160.29	2.79	97
GL8	Umm-Qasr	103.39	103.15	0.12	100
GL9	Umm-Qasr	78.64	77.87	0.49	100
GL10	Umm-Qasr	225.65	188.29	9.03	91
GL11	Umm-Qasr	241.59	209.73	7.06	93
GL12	Safwan-UmmQasr	136.04	132.29	1.40	99
GL13	Safwan-UmmQasr	132.96	113.28	7.99	92

Water quality

In this study, key parameters of EC, TDS, TH, and Cl^- were analyzed to evaluate the water type based on the salinity, water quality, and mineralization. The classification of water type according to the ranges of these parameters and the sample percentages were summarized in (Table 4). According to the salinity classification results, 100 % of samples represented high salinity water for EC exceeding 4000 µS/cm. Based on quality results classification, 46% of the samples were classified as saline water with EC values ranging from 1500 to10000 µS/cm, while 54% were classified as brine water with EC values exceeding 10000 µS/cm. Mineralization results indicated that 15% of the samples were moderately mineralized (EC 4000-6000 µS/cm), 31% were highly mineralized (EC 6000-10000 µS/cm), and 54% were excessively mineralized (EC >10000 µS/cm) as shown in Fig. 6a. According to Carroll (1962), 69% of the samples were classified as brackish water with TDS ranging from 1000 to 10000 mg/L, while 31% were classified as saline water with TDS ranging from 10000 to 100000 mg/L as shown in Fig. 6b. Based on the TH classification results, 100% of the samples were considered very hard water with TH exceeding 300 mg/L. Based on Stuyfzand (1989), 30.8% of the samples were classified as brackish water with Cl^- ranging from 300 to 1000 mg/L, and 69.2% were classified as brackish to saline water with Cl^- ranging from 1000 to 10000 mg/L.

Shah et al. (2019) noted that the chloride ion serves as an effective indicator of mixing phenomenon of ground-surface water, which causes fluctuations in the ionic content. However, the relationship between chloride concentration and electrical conductivity shows positive correlation (R^2 = 0.96) plotted in (Fig. 7). This indicates that higher Cl^- concentrations, often associated with seawater intrusion, lead to increased EC values in groundwater. According to Gimenez & Morell (1997), EC values exceeding 1000 µS/cm in coastal aquifers indicates seawater influence. However, identification of the salinization source is a more complicated issue; ionic ratios are largely used for identification the salinity in groundwater. It was highlighted by (Abdulameer et al., 2019; Al-Qurnawy et al., 2023). The ionic ratio Cl/HCO_3 is

Tab. 4 - Water classification based on EC, TDS, TH, and Cl^-.

Tab. 4 - Classificazione delle acque in base a EC, TDS, TH e Cl^-.

Parameter	References	Range	Water type	Samples %
EC (µS/cm) Salinity	Richard (1954) U.S. Salinity laboratory	250> 250-750 750-2250 2250-4000 4000<	Low Medium High Very high Extremely high	- - - - 100%
EC (µS/cm) Quality	Langenegger (1990)	333> 333-500 500-1100 1100-1500 1500-10000 10000<	Excellent Good Permissible Brackish Saline Brine	- - - - 46% 54%
EC (µS/cm) Mineralization	Detay (1997)	1000< 1000-2000 2000-4000 4000-6000 6000-10000 10000<	Very weak Weak Slight Moderate High Excessive	- - - 15% 31% 54%
TDS (mg/L)	Carroll (1962)	1000> 1000-10,000 10,000-100,000 100,000<	Fresh Brackish Saline Brine	- 69% 31% -
T.H (mg/L) as $CaCO_3$	Sawyer and McCarthy (1967)	75> 75-150 150-300 300<	Soft Moderately hard Hard Very hard	- - - 100%
Cl^- (mg/L)	Stuyfzand (1989)	<5 5-30 30-150 150-300 300-1000 1000-10000 10000-2000 20000<	Very Oligohaline Oligohaline fresh Fresh-brackish Brackish Brackish-salt Salt Hypersaline	- - - - 30.8% 69.2% - -

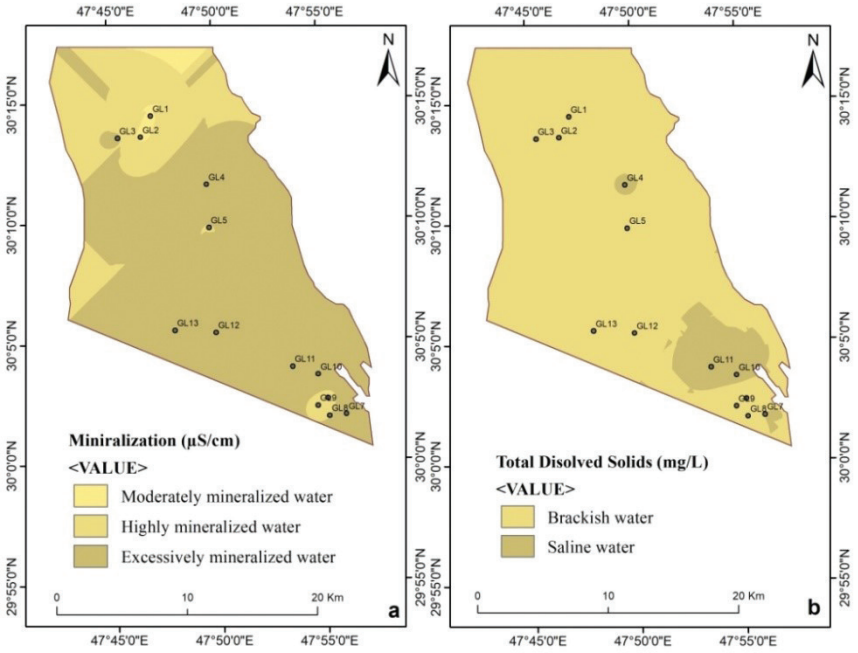

Fig. 6 - Spatial distribution maps (a) Mineralization, and (b) TDS.

Fig. 6 - Carte di distribuzione spaziale in riferimento (a) alla conducibilità elettrica e (b) ai solidi totali disciolti.

important factor for detecting seawater intrusion. This ratio is classified into six categories based on Todd (1959): less than 0.5: fresh water, 0.5-1.3; slightly contaminated 1.3-2.8; moderately contaminated 2.8-6.6; injuriously contaminated, 6.6-15.5; highly contaminated, and more than 15.5; severely contaminated. The Cl/HCO_3 ratio in groundwater samples ranged between 5.39 and 53.8 in molar concentrations (Fig 7b); 31% of the samples were classified as probably injuriously contaminated, 23% as highly contaminated, and 46% as severely contaminated. The SO_4/Cl values lower than unity indicate seawater mixing by domination of Cl^- over SO_4 (Abdalla, 2016; Abdulameer et al., 2018), whereas values greater than unity may represent dissolution of gypsum or contamination with fertilizers (Ghabayen et al., 2006). The SO_4/Cl ratio in groundwater ranged between 0.26 and 2.17 (Fig. 7c), with about 39% of the samples showing values below unity. A decrease in the Mg/Cl ratio with increasing Cl^- is most probably attributed to mixing with seawater (Batayneh et al., 2014). The Mg/Cl ratio ranged between 0.31 and 1.17 (Fig. 7d), with approximately 85% of the samples below unity. Therefore, groundwater in the study area is probably impacted by encroachment of seawater.

Piper Diagram

The Piper trilinear diagram uses the concentrations of cations and anions to interpret the geochemical evolution of saturated zone water. It is used for identifying the ionic species and the hydrochemical facies (Piper, 1944). The Piper diagram classifies the groundwater types into four facies based on the dominance of ions: Facies 1 ($Ca^{2+}Mg^{2+}$- Cl^- -SO_4^{2-} type), Facies 2 (Na^+- K^+- Cl^- -SO_4^{2-} type), Facies 3 (Na^+- K^+-HCO_3^- type), and Facies 4 (Ca^{2+}-Mg-HCO_3^- type). Within the study area, the chemical behavior of groundwater was assessed by analyzing the concentration of major cations (Ca^{2+}, Mg^{2+}, Na^+, and K^+) and major anions (HCO_3^-, SO_4^{2-}, and Cl^-) in

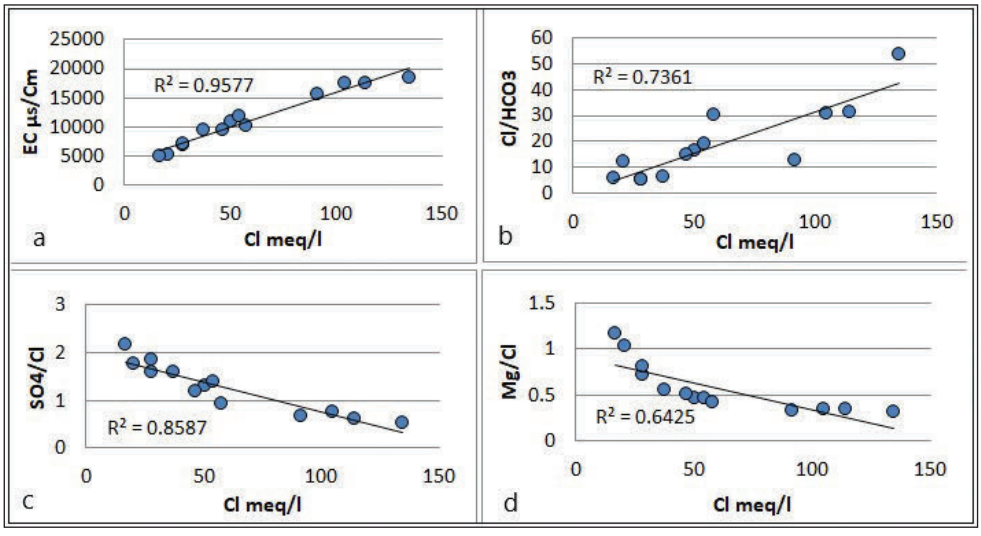

Fig. 7 - The chloride against electrical conductivity and ionic ratios in groundwater samples.

Fig. 7 - Correlazione tra cloruri e conducibilità elettrica nei campioni di acqua sotterranea

meq/L. According to the Piper plot, two subdivided chemical types have been observed: the Na-Cl (77%) and mixed Ca-Mg- Cl^- (23%) as shown in (Fig. 8). Most of the groundwater samples near the marine coasts have high content of sodium and chloride. As mentioned by Chandrasekar et al. (2014), calcium and bicarbonate are the dominant ions in freshwater whereas high concentrations in chloride and sodium in coastal groundwater are attributed to the seawater effect. Moreover, contaminated anthropogenic sources are considered as a factor for increasing salinity. Abdulameer et al. (2021) stated that sources of salinity in the concerned area mostly result from agricultural activities, including irrigation return flow, pesticides and fertilizers application to improved farmlands, as well as wastewater from septic tanks, industrial activities, desalination factories and gas storage stations, as well as the presence of an important port area.

Schoeller-Berkaloff Diagram

The Schoeller diagram is used for water quality assessment as drinking and agricultural usages (Baghvand et al., 2010). Figure 9 shows the Schoeller plot including the concentrations of cations (Ca^{2+}, Mg^{2+}, and Na^{+}) and anions (Cl, SO_4^{2-}, and HCO_3^{-}) in the groundwater. It is observed that the groundwater chemistry has essentially the same source, as indicated by the homogeneity in the direction, and the predominant sequence of the analyzed water samples was Cl^{-} >Na^{+} > SO_4^{2-} > Ca^{2+} > Mg^{2+} > HCO_3^{-}. This indicates that chloride, sodium and sulfate contents in some samples near the coast are relatively high compared to other samples such as GL1 and GL,2 in the upper part of the study area.

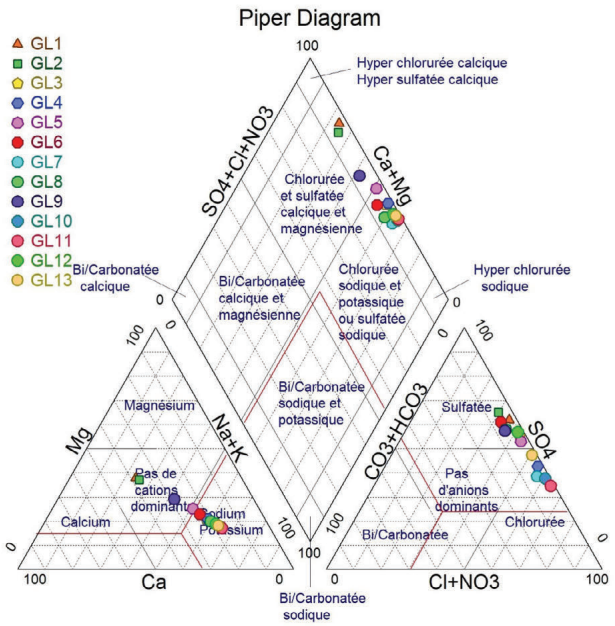

Fig. 8 - Piper diagram of groundwater samples.

Fig. 8 - Diagramma di Piper dei campioni di acqua sotterranea.

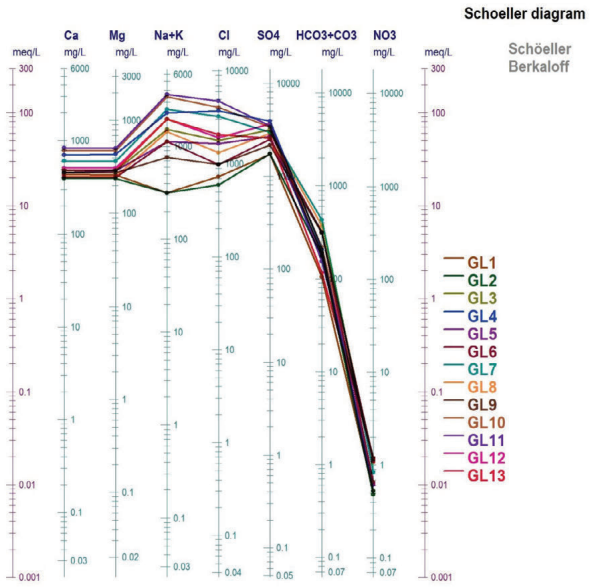

Fig. 9 - Schoeller Diagram of groundwater samples.

Fig. 9 - Diagramma di Schoeller dei campioni di acqua sotterranea.

Saturation indices

The saturation index detects the evolution of water chemistry and equilibrium state with the solid phases (Appelo and Postma, 2004). It provides valuable insights into geochemical processes by indicating dissolved and precipitated minerals in the water. The saturation index at a specific temperature can be defined using the following formula (2):

$$SI = \log\left(\frac{IAP}{Ks}\right) \quad (2)$$

where IAP represents the ion activity product of the mineral in water, and Ks is the solubility product of the mineral. Positive values of SI indicate supersaturation (precipitation), negative values of SI indicate undersaturation (dissolution), and SI values equal to 0 indicate equilibrium or saturation process between mineral and water. The saturation index of minerals in addition to the descriptive statistics of the analyzed water samples are summarized in (Tab. 5). The calcite $CaCO_3$ ranged from -0.01 to 0.68, with a mean value of 0.4, while dolomite $CaMg(CO_3)_2$ ranged from 0.07 to 1.47, with a mean value of 0.9. The gypsum $CaSO_4 \cdot 2H_2O$ varied from -0.23 to 0.05, averaging -0.12, while anhydrite $CaSO_4$ varied from -0.52 to -0.08, averaging -0.34. The halite NaCl differed from -5.43 to -3.56, with a mean value of -4.37, while sylvite KCl ranged from -6.35 to -5.37, mean -5.87. Figure 10 displays three cases of saturation indexes: slight precipitation of calcite and dolomite equilibrium to supersaturation state (SI<0), slight dissolution of gypsum and anhydrite under saturation state (SI>0), and strongly dissolution of halite and sylvite under saturation state (SI>0).

Tab. 5 - Results of saturation indices in groundwater samples based on PHREEQC.

Tab. 5 - Risultati degli indici di saturazione nei campioni di acqua sotterranea calcolati con PhreeqC.

Samples & statistics	Calcite ($CaCO_3$)	Dolomite $CaMg(CO_3)_2$	Gypsum $CaSO_4 \cdot 2H_2O$	Anhydrite $CaSO_4$	Halite NaCl	Sylvite KCl
GL1	0.07	0.24	-0.22	-0.49	-5.34	-6.35
GL2	0.15	0.39	-0.23	-0.52	-5.43	-6.18
GL3	-0.01	0.07	-0.08	-0.39	-4.3	-5.79
GL4	0.19	0.49	0.05	-0.22	-3.84	-5.37
GL5	0.18	0.48	-0.13	-0.41	-4.46	-5.85
GL6	0.48	1.07	-0.18	-0.45	-4.67	-6.01
GL7	0.68	1.47	-0.09	-0.37	-3.85	-5.7
GL8	0.58	1.26	-0.15	-0.42	-4.46	-6
GL9	0.63	1.37	-0.18	-0.43	-4.84	-6.04
GL10	0.63	1.38	-0.02	-0.2	-3.64	-5.45
GL11	0.63	1.39	-0.01	-0.08	-3.56	-5.6
GL12	0.53	1.14	-0.06	-0.15	-4.2	-5.91
GL13	0.41	0.91	-0.19	-0.28	-4.16	-6.05
Mean	0.396	0.897	-0.115	-0.34	-4.37	-5.87
Median	0.4800	1.070	-0.130	-0.39	-4.30	-5.91
S.D.	0.246	0.497	0.088	0.139	0.592	0.28
Minimum	-0.01	0.07	-0.23	-0.52	-5.43	-6.35
Maximum	0.68	1.47	0.05	-0.08	-3.56	-5.37

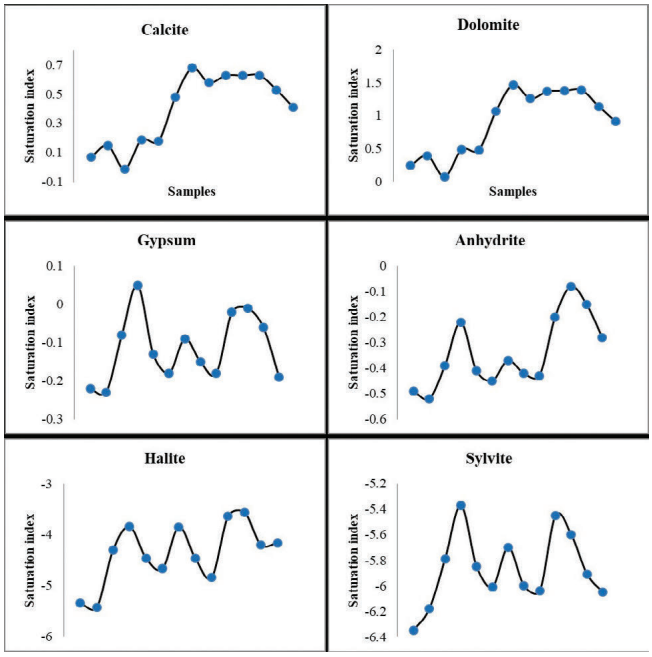

Fig. 10 - Saturation index of minerals in groundwater samples.

Fig. 10 - Indici di saturazione dei minerali nelle acque sotterranee.

The spatial distribution of saturation indices is delineated in (Fig. 11). The minimal precipitation to equilibrium of calcite (Fig. 11a) was identified in the southern part of the area. Dolomite (Fig. 11b) displayed similar behavior of calcite, but with higher values reflecting carbonate rocks and chemical weathering processes. The low solubility of gypsum and anhydrite in the groundwater (Fig. 11c, 11d) concentrated in the area indicates minimal dissolution of evaporite minerals. As mentioned by Mohanty & Rao. (2019), dissolution of gypsum can occur in the coastal groundwater. Furthermore, the sabkha deposits can produce dissolution of gypsum and anhydrite. The high solubility of halite in the groundwater (Fig. 11e) was concentrated in some samples in the southern part of the study area. Increased mineral solubility in groundwater may result from multiple sources including marine intrusion and surface contamination (El Mountassir & Bahir, 2023). Sylvite (Fig. 11f) also showed solubility in groundwater, which may involve evaporation from the ancient marine water or through fertilizer components, observed in the southern and eastern parts of the study area.

The coefficient of determination (R^2) between EC and SI of the six minerals described in (Fig. 12) shows that EC had a very weak correlation with calcite (R^2= 0.16%) and dolomite (R^2= 0.17%). On the other side, EC had a strong negative correlation with gypsum (R^2= 0.85%), moderate negative correlation with anhydrite (R^2= 0.70%), and very strong negative correlation with halite (R^2= 0.91%) and sylvite (R^2= 0.86%).

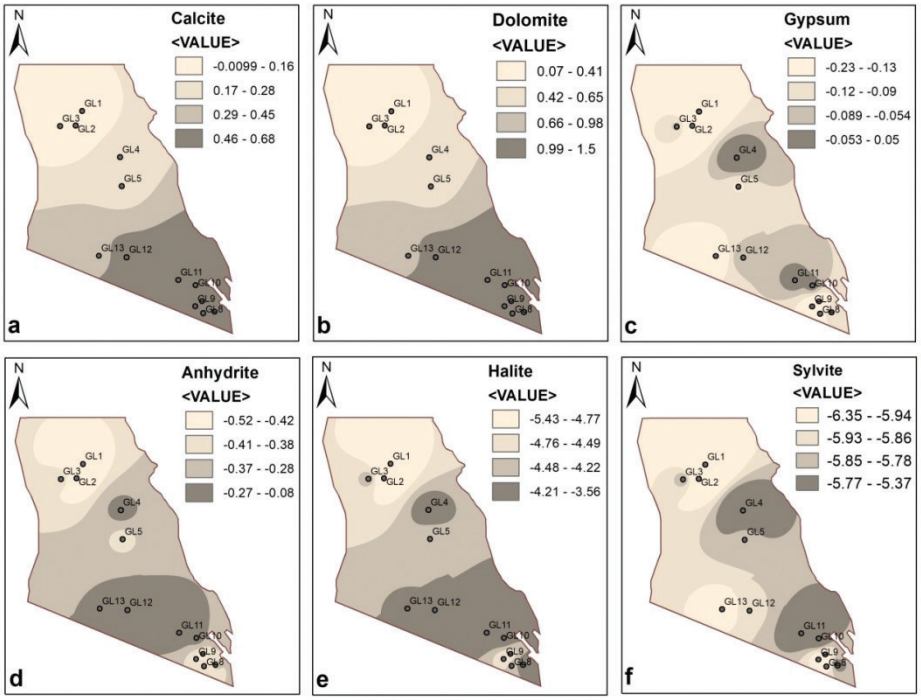

Fig. 11 - Spatial distributions of saturation indices of minerals in groundwater samples.

Fig. 11 - Distribuzione spaziale degli indici di saturazione dei minerali nei campioni di acqua sotterranea.

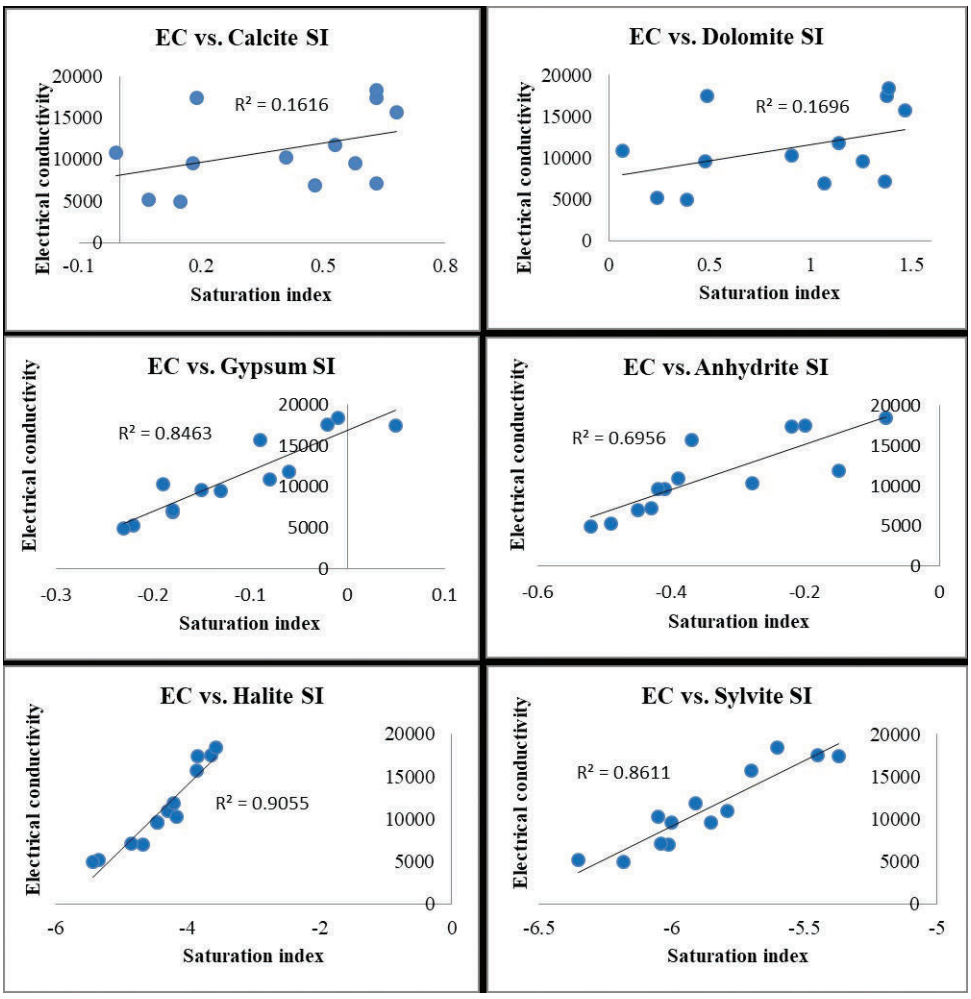

Fig. 12 - Saturation index of minerals vs. EC in groundwater samples.

Fig. 12 - Indice di saturazione dei minerali in funzione della conducibilità elettrica nei campioni di acqua sotterranea.

Gibbs plots

As mentioned by Zhang et al. (2024), Gibbs (1970) determined the sources of coastal groundwater based on three processes, evaporation, precipitation, and rock-water interaction, using two ratios Na/Na+Ca and Cl/Cl+HCO_3, plotted against TDS. The summary statistics of the Gibbs ratios are given in (Tab. 6). In the context of the study area, the Na/(Na+Ca) ratio ranged from 0.413 to 0.812, with a mean value of 0.71, while the Cl/(Cl+HCO_3) ratio ranged from 0.758 to 0.969, with a mean value of 0.87.

Tab. 6 - The summary statistics of the Gibbs ratio in the groundwater samples.

Tab. 6 - Statistiche sintetiche del rapporto di Gibbs nei campioni di acqua sotterranea.

Parameter	Mean	Median	S.D	Minimum	Maximum
Gibbs Na/Na+Ca	0.709	0.762	0.138	0.413	0.812
Gibbs Cl/Cl+HCO_3	0.874	0.897	0.079	0.758	0.969

As observed by Figure 13a, 13b, the groundwater in the area was primarily affected by the processes of seawater and evaporation dominance. Most of analyzed water samples exhibit ratio values greater than 0.6, suggesting that those processes play a more significant role in the aquifer than the rock-water interactions and precipitation dominance. In addition to the increasing salinity of groundwater as stated by El-Rawy et al (2023), other factors - including seawater intrusion, high evaporation process within the arid area and returned irrigated water from farming lands - also contribute to the high salinization.

Cluster analysis

The cluster analysis represents a powerful statistical tool that is widely used for identifying the chemical constituents that affect the groundwater quality (Hasan et al., 2023). Hydrochemical studies applied hierarchical cluster analysis to classify samples into hydrochemical clusters (subgroups) represented as dendrograms based on similarity in characteristics (Benaafi et al., 2023), which depend on groundwater characteristics, geological formations, human-induced impacts, and climate change (Bellaredj, 2025). Groundwater samples under the investigated area are subjected to the hierarchical cluster analysis using Euclidean distance method. Figure 14 shows the dendrogram involving three main groups (cases) categorized based on similarity and proximity to one another. The first (upper) group includes samples (GL10, GL11, GL13, GL4, and GL7) and is characterized by the high chemical composition and salinity. The second group includes samples (GL3, GL5, GL8, GL12, GL6, and GL9), and then the third lowest group, which is represented by the two samples (GL1, and GL2) with the lowest level of chemical composition. However, cluster analysis identified four distinct groups reflecting composition of groundwater and hydrochemical processes (Fig. 15); the first cluster was dominated by Ca^{2+}- TH - Mg^{2+}, the second by EC- TDS - Na^{+}- Cl^{-}, the third by SO_4^{2-}, and fourth cluster by HCO_3^{-} - NO_3^{-}- K^{+}. Groups 2 and 3 are characterized by high EC, TDS, Na^{+}, Cl^{-}, and SO_4^{2-} concentrations and correspond to seawater intrusion with reverse ion exchange and high salinity, while group 1 represents a transitional mixing zone influenced by mineral dissolution and ion exchange processes (Athauda et al., 2024). The presence of HCO_3^{-} and NO_3^{-} in group 4 indicates natural groundwater characteristics and potential anthropogenic input (El Mountassir and Bahir, 2023). HCO_3^{-} reflect recharge from rainfall (Abusalem et al., 2022), which is consistent with sampling during winter, when rainfall likely contributed to the aquifer. HCO_3^{-} is more abundant in freshwater and minimal in seawater, in contrast with Cl (Bourjila et al., 2024). Although fertilizers applied in agricultural lands can contribute NO_3^{-} to groundwater (Rajendiran et al., 2021), nitrate contamination in the current study is insignificant due to the low concentrations observed.

Conclusions:

The present study investigates seawater intrusion into groundwater in the Dibdibba coastal aquifer, southeast of Basrah, southern Iraq, using the hydrochemical technique, geochemical modeling, and statistical analysis. Critical points can be concluded from this study as follows;

The groundwater properties in the selected area were slightly alkaline and very hard based on pH and total hardness. From the quality classification, the groundwater

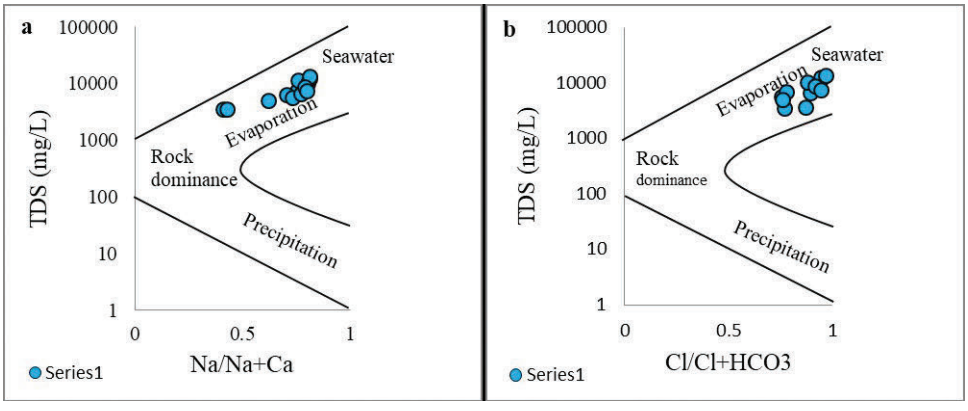

Fig. 13 - Gibbs plots showing TDS against (a) cations, (b) anions.

Fig. 13 - Diagrammi di Gibbs che mostrano la relazione tra i solidi totali disciolti (TDS) e (a) i cationi, (b) gli anioni.

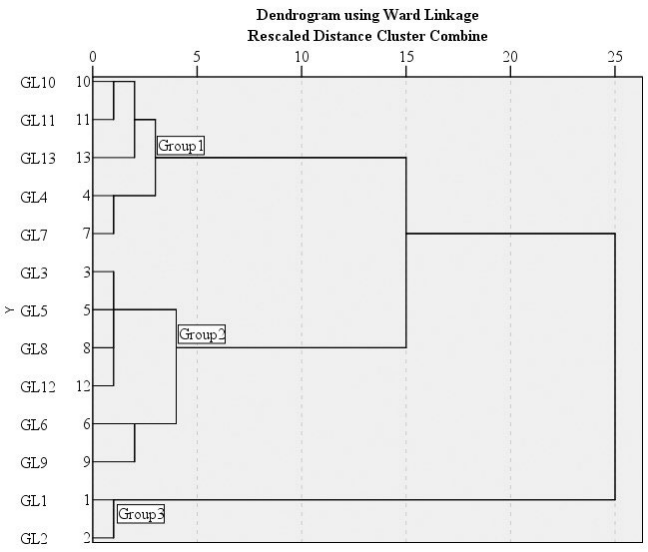

Fig. 14 - Dendrogram of hierarchical cluster analysis declaring grouping of samples (cases) based on similarity and proximity of physicochemical parameters.

Fig. 14 - Dendrogramma dell'analisi gerarchica dei cluster che evidenzia il raggruppamento dei campioni in base alla similarità e alla prossimità dei parametri fisico-chimici.

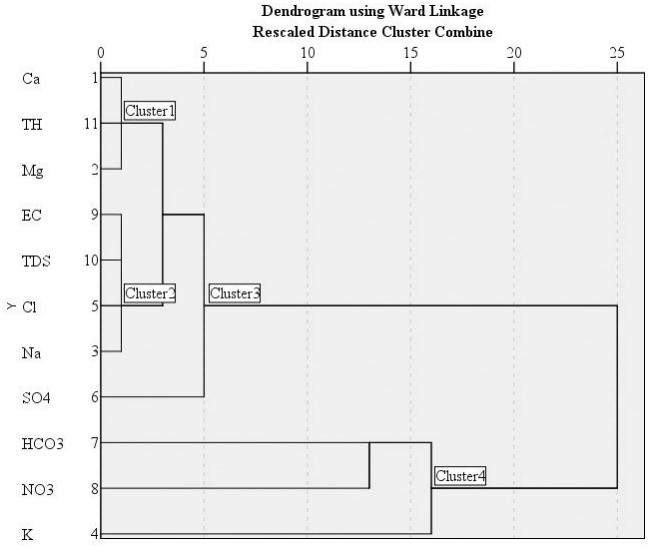

Fig. 15 - Dendrogram of hierarchical cluster analysis declaring physicochemical parameters (variables).

Fig. 15 - Dendrogramma dell'analisi gerarchica dei cluster relativo ai parametri fisico-chimici (variabili).

exhibited extremely high salinity, ranged from saline to brine quality, and showed moderate to excessive mineralization.

According to Piper diagram, the origin of groundwater under the selected investigation is distributed within two hydrochemical facies: the Na–Cl and Ca–Mg–Cl. As indicated by Schoeller diagram, the predominant sequence of the groundwater followed the order Cl^- > Na^+ >SO_4^{2-}> Ca^{2+} > Mg^{2+}> HCO_3^- indicating high levels of Cl^-, Na^+, and SO_4^{2-}. Based on the saturation indices of minerals, slight precipitation of calcite and dolomite in the groundwater suggests stable circumstances in water chemistry. Moreover, minimal dissolution of gypsum and anhydrite, and high dissolution of halite and sylvite were strongly correlated with the salinity. According to Gibbs plots, the groundwater chemistry was governed by seawater mixing, and evaporation dominance, probably from up-coning saline deeper water. Additionally, the hierarchical cluster analysis revealed four groups of groundwater: Ca^{2+}-TH-Mg^{2+} involving mineral dissolution and ion exchange processes, EC-TDS-Na^+-Cl^- and SO_4^{2-} reflecting seawater intrusion and reverse ion exchange due to the high salinity representing this group, and HCO_3^--NO_3^--K^+ indicates natural groundwater chemistry impacted by agricultural and anthropogenic activities.

This informative work provides valuable information for decision makers and planners for enhancing the protection of groundwater from salinization and emphasizing the need for sustainable groundwater policies in the arid coastal regions.

Author contributions

Conceptualization: Lamees Al-Qurnawy; Methodology: Lamees Al-Qurnawy; interpretation of results: Lamees Al-Qurnawy; visualization: Lamees Al-Qurnawy and Wisam Muttashar; Writing original draft preparation: Lamees Al-Qurnawy; Supervision: Wisam Muttashar and Ali Al-Ansari. All authors read and approved the final manuscript.

Competing interest

The author declare no competing interest.

Additional information

DOI: https://doi.org/10.7343/as-2025-917

REFERENCES

Abdalla, F. (2016). Ionic ratios as tracers to assess seawater intrusion and to identify salinity sources in Jazan coastal aquifer, Saudi Arabia. Arabian Journal of Geosciences, 9(1), 1-12. https://doi.org/10.1007/s12517-015-2065-3

Abdulameer, A., Thabit, J. M., AL-Menshed, F. H., & Merkel, B. (2018). Investigation of seawater intrusion in the Dibdibba Aquifer using 2D resistivity imaging in the area between Al-Zubair and Umm Qasr, southern Iraq. Environmental Earth Sciences, 77, 1-15. https://doi.org/10.1007/s12665-018-7798-3.

Abdulameer, A., Thabit, J. M., Kanoua, W., Wiche, O., & Merkel, B. (2021). Possible sources of salinity in the upper Dibdibba aquifer, Basrah, Iraq. Water, 13(4), 578. https://doi.org/10.3390/w13040578.

Al Naqib, K. M. (1967). Geology of the Arabian Peninsula:. United States Department of the Interior, Geological Survey. https://doi.org/10.3133/pp560G.

Aladejana, J. A., Kalin, R. M., Sentenac, P., & Hassan, I. (2021). Groundwater quality index as a hydrochemical tool for monitoring saltwater intrusion into coastal freshwater aquifer of Eastern Dahomey Basin, Southwestern Nigeria. Groundwater for Sustainable Development, 13, 100568. https://doi.org/10.1016/j.gsd.2021.100568.

Alfarrah, N., & Walraevens, K. (2018). Groundwater overexploitation and seawater intrusion in coastal areas of arid and semi-arid regions. Water, 10(2), 143. https://doi.org/10.3390/w10020143.

Al-Jawad, S. B., Ayob, M. S., Khalil, S., & Al-Radi, N. H. (1989). Hydraulic properties of Dibdibba sandstone using pumping tests data in large diameter wells. In Proc. 5th, Sci., Conf., SRC., Iraq (Vol. 3, No. 3, pp. 133-146).

Al-Jiburi, H. K., & Al-Basrawi, N. H. (2009). Hydrogeology. IRAQI BULLETIN OF GEOLOGY AND MINING, (2), 77-91.

Al-Kubaisi, Q. Y. (1996). Hydrogeology of Dibdiba Aquifer in Safwan–Zubair area, South Iraq. Unpublished Ph. D. Thesis, University of Baghdad, Baghdad.

Al-Kubaisi, Q. Y. (1999). Quaternary-Tertiary hydrogeologic boundary condition at Safwan-Zubair area. South of Iraq. Iraq Jour Sci, 40(3), 21-28.

Al-Mallah, I. A., Al-Qurnawi, W. S., Ghalib, H. B., Al Hawash, A. B., & Abdulameer, M. H. (2022). Evaluation of groundwater quality in the Dibdibba aquifer using hydrogeochemical and isotope techniques (Basrah Province, Iraq). Acta Geochimica, 41(5), 823-838. https://doi.org/10.1007/s11631-022-00549-8

Al-Musawi, W. M., & Khorshid, S. Z. (2013). Determination of the saline water intrusion zone and its contamination with ground water in the Dibddiba aquifer using vertical electrical sounding technique at Basrah Governorate, southern Iraq. Mesopotamian Journal of Marine Sciences, 28(2), 93-108.

Alqurnawy, L. S., Almallah, I. A., & Alrubaye, A. (2022). Groundwater vulnerability analysis via GALDIT-GIS method to seawater intrusion, South of Iraq. The Iraqi Geological Journal, 146-161. https://doi.org/10.46717/igj.55.1E.12Ms-2022-05-28.

Al-Qurnawy, L. S., Almallah, I. A., & Alrubaye, A. (2023, July). Identification of seawater intrusion in the dibdibba coastal aquifer, south of Iraq using chemical indicators and multivariate analyses. In IOP Conference Series: Earth and Environmental Science (Vol. 1215, No. 1, p. 012054). IOP Publishing. https://doi.org/10.1088/1755-1315/1215/1/012054.

Al-Qurnawy, L., Almallah, I. A., & Alrubaye, A. (2024). Hydrochemical Characteristics and Spatial Variability in Coastal Aquifers Southern IraqUtilizing a GIS Technique. The Iraqi Geological Journal, 264-276. https://doi.org/10.46717/igj.57.2C.18ms-2024-9-26

Al-Ramadhan, B. M. (1988). Residual fluxes of water in an estuarine lagoon. Estuarine, Coastal and Shelf Science, 26(3), 319-330. https://doi.org/10.1016/0272-7714(88)90068-6

Al-Sudani, H. I. Z. (2019). Groundwater system of Dibdibba sandstone aquifer in south of Iraq. Applied Water Science, 9(4), 72. https://doi.org/10.1007/s13201-019-0952-6

Al-Suraifi, A. A. A. Groundwater and Seawater Intrusion Simulation at Basrah Coastal Aquifer (Aug. 2015). In The 2nd International Conference of Buildings, Construction and Environmental Engineering (BCEE2-2015) (p. 63).

Appelo, C. A. J., & Postma, D. (2004). Geochemistry, groundwater and pollution. CRC press.

Ardjane, T. A., Meddah, B., Bekkoussa, B. S., Zemour, K., & Mairif, M. (2025). Groundwater quality assessment using water quality index coupled with multivariate statistical analysis in the alluvial plains of El-Abd and El-That, Tiaret Region, Northwestern Algeria. Acque Sotterranee-Italian Journal of Groundwater, 14(2). https://doi.org/10.7343/as-2025-852

Athauda, S., Wang, Y., Hao, Z., Indika, S., Yapabandara, I., Weragoda, S. K., ... & Wei, Y. (2024). Geochemical assessment of the evolution of groundwater under the impact of seawater intrusion in the Mannar district of Sri Lanka. Water, 16(8), 1137. https://doi.org/10.3390/w16081137

Atiaa, A. M. (2000). Hydrogeology of Safwan-Zubair area, south of Iraq, Unpub (Doctoral dissertation, M. Sc. Thesis, College of Scaince, University of Basrah, 90p).

Atiaa, A. M., & Al-Asadiy, S. A. A. A. (2007). Management of Groundwater Reseource of Dibdibba Sandy Aquifer in Safwan-Zubair Area, South of Iraq. Journal of the College of Arts. University of Basrah No, 42, 200

Baghvand, A., Nasrabadi, T., Bidhendi, G. N., Vosoogh, A., Karbassi, A., & Mehrdadi, N. (2010). Groundwater quality degradation of an aquifer in Iran central desert. Desalination, 260(1-3), 264-275. http://dx.doi.org/10.1016/j.desal.2010.02.038.

Batayneh, A., Zaman, H., Zumlot, T., Ghrefat, H., Mogren, S., Nazzal, Y., ... & Al-Taani, A. (2014). Hydrochemical facies and ionic ratios of the coastal groundwater aquifer of Saudi Gulf of Aqaba: implication for seawater intrusion. Journal of Coastal Research, 30(1), 75-87.

Bellaredj, A. E. M. (2025). Groundwater quality assessment for drinking and irrigation in the plains of Oran (northwestern Algeria) using geographic information system, water quality indices and multivariate statistical methods. Acque Sotterranee-Italian Journal of Groundwater, 14(3). htpps://doi.org/10.7343/as-2025-878

Benaafi, M., Abba, S. I., Tawabini, B., Abdulazeez, I., Salhi, B., Usman, J., & Aljundi, I. H. (2023). Integrated clustering analysis for delineating seawater intrusion and heavy metals in Arabian Gulf Coastal groundwater of Saudi Arabia. Heliyon, 9(9). https://doi.org/10.1016/j.heliyon.2023.e19784.

Bourjila, A., Dimane, F., Ghalit, M., Taher, M., Kamari, S., El Hammoudani, Y., ... & Benaabidate, L. (2024). Exploring salinity origins in the Ghiss-Nekor aquifer, northern Morocco: A multivariate statistical analysis. In BIO Web of Conferences (Vol. 109, p. 01017). EDP Sciences. https://doi.org/10.1051/bioconf/202410901017

Buday, T. (1980). The regional geology of Iraq, stratigraphy and paleotology. Som Dar Alkitab publishing house, Mosul, 445p.

Carroll, D. (1962). Rainwater as a chemical agent of geology processes.

Chandrasekar, N., Selvakumar, S., Srinivas, Y., John Wilson, J. S., Simon Peter, T., & Magesh, N. S. (2014). Hydrogeochemical assessment of groundwater quality along the coastal aquifers of southern Tamil Nadu, India. Environmental earth sciences, 71, 4739-4750. https://doi.org/10.1007/s12665-013-2765-2.

Detay, M. (1997). Water wells: implementation, maintenance and restoration. JOHN WILEY & SONS, CHICHESTER(UK). 379, 1997.

El Mountassir, O., & Bahir, M. (2023). The assessment of the groundwater quality in the coastal aquifers of the Essaouira Basin, Southwestern Morocco, using hydrogeochemistry and isotopic signatures. Water, 15(9), 1769. https://doi.org/10.3390/w15091769

El-Rawy, M., Fathi, H., Abdalla, F., Alshehri, F., & Eldeeb, H. (2023). An integrated principal component and hierarchical cluster analysis approach for groundwater quality assessment in Jazan, Saudi Arabia. Water, 15(8), 1466. https://doi.org/10.3390/w15081466.

Ghabayen, S. M., McKee, M., & Kemblowski, M. (2006). Ionic and isotopic ratios for identification of salinity sources and missing data in the Gaza aquifer. Journal of hydrology, 318(1-4), 360-373. https://doi.org/10.1016/j.jhydrol.2005.06.041

Ghalib, H. B. (2000). Hydrogeochemistry and effect of pumping on the groundwater quality of Dibdabba aquifer in Safwan-Zubair Area (Southern Iraq) (Doctoral dissertation, MSc Thesis, University of Basrah).

Ghalib, H. B. (2008). Simulation Study of the effect of artificial recharge on the water quality of shallow Dibdibba Clastic Aquifer in Zubair-Safwan area, south of Iraq. Journal Basrah Researches (Sciences), 34(4), 47-57.

Gibbs, R. J. (1970). Mechanisms controlling world water chemistry. Science, 170(3962), 1088-1090.

Gimenez, E., & Morell, I. (1997). Hydrogeochemical analysis of salinization processes in the coastal aquifer of Oropesa (Castellon, Spain). Environmental geology, 29, 118-131.

Haddad, R. H., & Hawa, A. J. (1979). Hydrogeology of the Safwan-Zubair area, south of Iraq. Tech. Bull, 132.

Hasan, S. S., Salem, Z. E., & Sefelnasr, A. (2023). Assessment of hydrogeochemical characteristics and seawater intrusion in coastal aquifers by integrating statistical and graphical techniques: quaternary Aquifer, West Nile Delta, Egypt. Water, 15(10), 1803. https://doi.org/10.3390/w15101803.

Hassan, Z. D. (2025). Geomorphological and Environmental Characteristics of the Al-Mashab and Al-Salal Marshes, Southern Iraq. Iraqi Journal of Science.
https://doi:10.24996/ijs.2025.66.3.10

IBM Corp, N. (2017). IBM SPSS statistics for windows. Version 25.0.

Jassim, S. Z., & Goff, J. C. (Eds.). (2006). Geology of Iraq. DOLIN, sro, distributed by Geological Society of London.

Kanagaraj, G., Elango, L., Sridhar, S. G. D., & Gowrisankar, G. (2018). Hydrogeochemical processes and influence of seawater intrusion in coastal aquifers south of Chennai, Tamil Nadu, India. Environmental Science and Pollution Research, 25, 8989-9011. https://doi.org/10.1007/s11356-017-0795-0.

Langenegger, O. (1990). Groundwater quality in rural areas of Western Africa. In Sahel forum. The state-of-the-art of hydrology and hydrogeology in the arid and semi-arid areas of Africa (pp. 574-584).

McArthur, J. M., Turner, J., Lyons, W. B., & Thirlwall, M. F. (1989). Salt sources and water-rock interaction on the Yilgarn Block, Australia: isotopic and major element tracers. Applied Geochemistry, 4(1), 79-92. https://doi.org/10.1016/0883-2927(89)90060-7.

Mohanty, A. K., & Rao, V. G. (2019). Hydrogeochemical, seawater intrusion and oxygen isotope studies on a coastal region in the Puri District of Odisha, India. Catena, 172, 558-571. https://doi.org/10.1016/j.catena.2018.09.010.

Muttashar, W. R., Al-Aesawi, Q. M., Al-Nasrawi, A. K., Almayahi, D. S., & Jones, B. G. (2024). Coastline instability evaluation: multitemporal bathymetric mapping and sediment characteristics. Environmental Earth Sciences, 83(1), 43. https://doi.org/10.1007/s12665-024-10962-4.

Parkhurst, D. L., & Appelo, C. A. J. (2013). Description of input and examples for PHREEQC version 3-a computer program for speciation, batch-reaction, one-dimensional transport, and inverse geochemical calculations. US geological survey techniques and methods, 6(A43), 497. https://pubs.usgs.gov/tm/06/a43/

Piper, A. M. (1944). A graphic procedure in the geochemical interpretation of water-analyses. Eos, Transactions American Geophysical Union, 25(6), 914-928.

Rajendiran, T., Sabarathinam, C., Chandrasekar, T., Panda, B., Mathivanan, M., Nagappan, G., ... & Alagappan, R. (2021). Geochemical variations due to salinization in groundwater along the southeast coast of India. SN Applied Sciences, 3(5), 581. https://doi.org/10.1007/s42452-021-04551-2

Richards, L. A. (Ed.). (1954). Diagnosis and improvement of saline and alkali soils (No. 60). US Government Printing Office.

Samsudin, A. R., Haryono, A., Hamzah, U., & Rafek, A. G. (2008). Salinity mapping of coastal groundwater aquifers using hydrogeochemical and geophysical methods: a case study from north Kelantan, Malaysia. Environmental Geology, 55(8), 1737-1743. http://dx.doi.org/10.1007/s00254-007-1124-9.

Sarikhani, R., Ghassemi Dehnavi, A., Ahmadnejad, Z., & Kalantari, N. (2015). Hydrochemical characteristics and groundwater quality assessment in Bushehr Province, SW Iran. Environmental Earth Sciences, 74, 6265-6281. https://doi.org/10.1007/s12665-015-4792-5.

Sawyer, C. N., & McCarty, P. L. (1967). Chemistry for sanitary engineers.

Selvam, S., Manimaran, G., & Sivasubramanian, P. (2013). Hydrochemical characteristics and GIS-based assessment of groundwater quality in the coastal aquifers of Tuticorin corporation, Tamilnadu, India. Applied Water Science, 3, 145-159. https://doi.org/10.1007/s13201-013-0122-3.

Shah, B., Kansara, B., Shankar, J., Soni, M., Bhimjiyani, P., Bhanushali, T., ... & Sircar, A. (2019). Reckoning of water quality for irrigation and drinking purposes in the konkan geothermal provinces, Maharashtra, India. Groundwater for sustainable development, 9, 100247. https://doi.org/10.1016/j.gsd.2019.100247.

Simler, R. (2009). DIAGRAMMES: Logiciel d'hydrochimie multilangage en distribution *"Multilingual hydrochemistry software in distribution"*.

Sissakian, V. K., & Fouad, S. F. (2015). Geological map of Iraq, scale 1: 1000 000, 2012. Iraqi Bulletin of Geology and Mining, 11(1), 9-16.

Sissakian, V. K., & Mohammed, B. S. (2007). Stratigraphy. Iraqi Bulletin of Geology and Mining, (1), 51-124.

Sissakian, V. K., Shihab, A. T., Al-Ansari, N., & Knutsson, S. (2014). Al-Batin alluvial fan, southern Iraq. Engineering, 6(11), 699-711.

Stuyfzand, P. J. (1989). A new hydrochemical classification of water types. Iahs Publ, 182, 89-98.

Todd, DK. (1959). Groundwater hydrology. United States. John Wiley and Sons. Inc.pp 277-294

Tomaszkiewicz, M., Abou Najm, M., & El-Fadel, M. (2014). Development of a groundwater quality index for seawater intrusion in coastal aquifers. Environmental Modelling & Software, 57, 13-26. https://doi.org/10.1016/j.envsoft.2014.03.014.

Zhang, M. H., Zhou, S. Y., Liu, D. D., Zhang, Y., Zhang, Y. X., Chen, X., ... & Shi, W. P. (2024). Characteristics and genesis of groundwater salinization in coastal areas of the Lower Reaches of Oujiang Basin. Journal of Groundwater Science and Engineering, 12(2), 190-204. https://doi.org/10.26599/JGSE.2024.9280015